mTORC1 inhibition restricts inflammation-associated gastrointestinal tumorigenesis in mice

Stefan Thiem,[1] Thomas P. Pierce,[1] Michelle Palmieri,[1] Tracy L. Putoczki,[1] Michael Buchert,[1] Adele Preaudet,[1] Ryan O. Farid,[1] Chris Love,[1] Bruno Catimel,[1] Zhengdeng Lei,[2] Steve Rozen,[2] Veena Gopalakrishnan,[3] Fred Schaper,[4] Michael Hallek,[5] Alex Boussioutas,[6] Patrick Tan,[3] Andrew Jarnicki,[1] and Matthias Ernst[1]

[1]Ludwig Institute for Cancer Research, Melbourne-Parkville Branch, Parkville, Victoria, Australia. [2]Neuroscience and Behavioral Disorder Program and [3]Cancer and Stem Cell Biology Program, Duke-NUS Graduate Medical School, Singapore. [4]Institut für Biologie, Otto-von-Guericke-Universität, Magdeburg, Germany. [5]Klinik I für Innere Medizin, Uniklinik Köln, Köln, Germany. [6]Peter MacCallum Cancer Centre, Melbourne, Victoria, Australia.

Gastrointestinal cancers are frequently associated with chronic inflammation and excessive secretion of IL-6 family cytokines, which promote tumorigenesis through persistent activation of the GP130/JAK/STAT3 pathway. Although tumor progression can be prevented by genetic ablation of *Stat3* in mice, this transcription factor remains a challenging therapeutic target with a paucity of clinically approved inhibitors. Here, we uncovered parallel and excessive activation of mTOR complex 1 (mTORC1) alongside STAT3 in human intestinal-type gastric cancers (IGCs). Furthermore, in a preclinical mouse model of IGC, GP130 ligand administration simultaneously activated mTORC1/S6 kinase and STAT3 signaling. We therefore investigated whether mTORC1 activation was required for inflammation-associated gastrointestinal tumorigenesis. Strikingly, the mTORC1-specific inhibitor RAD001 potently suppressed initiation and progression of both murine IGC and colitis-associated colon cancer. The therapeutic effect of RAD001 was associated with reduced tumor vascularization and cell proliferation but occurred independently of STAT3 activity. We analyzed the mechanism of GP130-mediated mTORC1 activation in cells and mice and revealed a requirement for JAK and PI3K activity but not for GP130 tyrosine phosphorylation or STAT3. Our results suggest that GP130-dependent activation of the druggable PI3K/mTORC1 pathway is required for inflammation-associated gastrointestinal tumorigenesis. These findings advocate clinical application of PI3K/mTORC1 inhibitors for the treatment of corresponding human malignancies.

Introduction

During the multistep process of tumor formation conditions within the tissue microenvironment can influence the fate of premalignant cells. In inflammation-associated cancers, tumor promotion is thought to be facilitated by the interaction of initiated epithelial cells, which harbor mutations in proto-oncogenes or tumor suppressor genes, with a microenvironment rich in growth-promoting inflammatory mediators. These mediators activate mitogenic pathways that trigger the expansion of premalignant clones (1). In gastrointestinal tumorigenesis, evidence for the tumor-promoting role of inflammation comes from positive clinical correlations between inflammatory bowel disease and colorectal cancer incidence (2, 3) and the success of antiinflammatory medications in suppressing colorectal malignancies (4, 5). Although the precise molecular mechanisms that link inflammation to epithelial tumor promotion may vary between cancers, most inflammation-associated signaling pathways converge on a number of key regulators in tumor cells, including the transcription factors STAT3 and NF-κB (1). Therapeutic inhibition of these growth- and survival-promoting pathways represents a promising strategy to inhibit the development of inflammation-associated malignancies.

Aberrant activation of STAT3 is a unifying hallmark of inflammation-associated cancers (1). Excessive STAT3 activity promotes proliferation of neoplastic cells through transcriptional induction of c-Myc and cyclin D1, D2, and B and simultaneously upregulates cell survival mediators, including Bcl-2, Bcl-X, and survivin (6, 7). Intriguingly, persistent STAT3 activation frequently occurs in the absence of activating mutations in, or amplification of, the *STAT3* gene. Instead, STAT3 activation commonly coincides with an abundance of tumor and stromal cell–derived cytokines that characterize the tumor microenvironment (1, 7). Among these are IL-6 and IL-11, 2 IL-6 family cytokines that share the common receptor subunit GP130 and signal via JAK-mediated activation of STAT3 (8). Both cytokines have been identified, through genetic and pharmacologic manipulations in mice, as promising therapeutic targets for gastrointestinal and hepatic cancers (9–11).

We have previously characterized the $gp130^{Y757F/Y757F}$ (hereafter referred to as $gp130^{FF}$) mouse as a robust model for inflammation-associated gastric tumorigenesis, in which disease arises from excessive GP130/STAT3 activation in response to IL-6 family cytokines (12, 13). Homozygous $gp130^{FF}$ mice spontaneously and reproducibly develop tumors in the most distal part of the glandular stomach by 4 weeks of age. Tumor development is prevented by systemic restriction of *Stat3* expression in $gp130^{FF}Stat3^{+/-}$ mice or by the absence of

Conflict of interest: The authors have declared that no conflict of interest exists.

Note regarding evaluation of this manuscript: Manuscripts authored by scientists associated with Duke University, The University of North Carolina at Chapel Hill, Duke-NUS, and the Sanford-Burnham Medical Research Institute are handled not by members of the editorial board but rather by the science editors, who consult with selected external editors and reviewers.

Citation for this article: *J Clin Invest.* doi:10.1172/JCI65086.

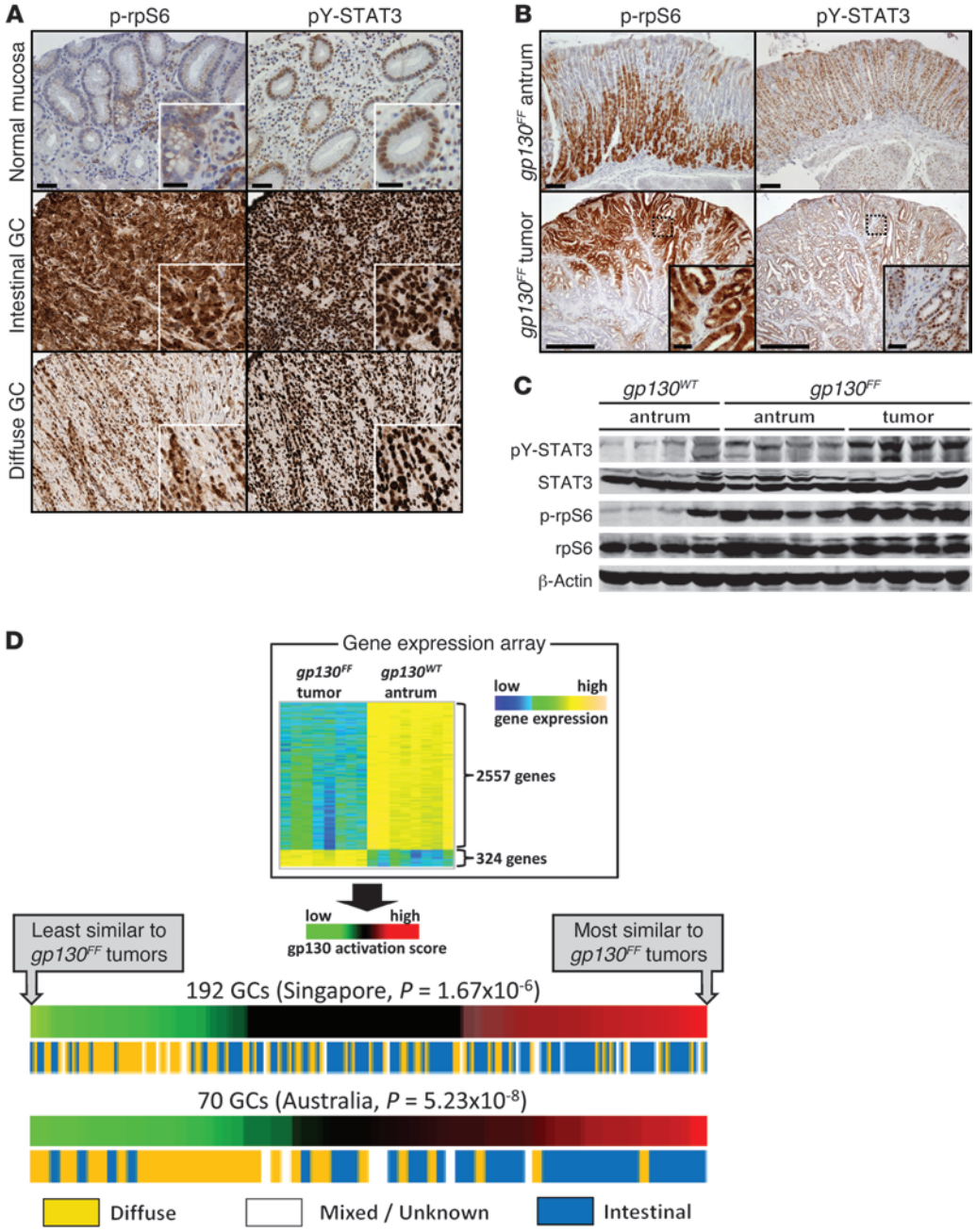

Figure 1
Coactivation of mTORC1 and STAT3 in gastric tumors of humans and *gp130*^{FF} mice. (**A** and **B**) Representative immunostaining for serine-phosphorylated ($S_{240/244}$) rpS6 and tyrosine-phosphorylated (Y_{705}) STAT3 on biopsy sections of (**A**) normal human gastric mucosa and GC or (**B**) unaffected antra and tumors from *gp130*^{FF} mice. Scale bar: 500 μm; 50 μm (insets). Also refer to Supplemental Figure 1. Higher-magnification images (insets) demonstrate staining of neoplastic epithelial cells. (**C**) Immunoblot analysis for pY-STAT3 and p-rpS6 of unaffected antra and pooled tumors from individual mice of the indicated genotype. (**D**) Correlation of the gene expression profile between *gp130*^{FF} mouse tumors and human IGC. Heat map of differentially expressed genes between *gp130*^{FF} tumors and antral mucosa of wild-type mice (*gp130*^{WT} mice) (top). The human orthologs of these genes were used to calculate a human GP130 activation score for individual expression signatures of GC biopsies collected in Singapore or Australia (bottom). The panels depict the correlation between the GP130 activation score of each biopsy and their histological classification according to the report by Lauren (21). Also refer to Supplemental Table 1.

the ligand-binding IL-11 receptor α (*Il11ra*) subunit in compound *gp130*^{FF}*Il11ra*$^{-/-}$ mice but not by *Il6* gene ablation (10). Similarly, therapeutic inhibition of STAT3 or IL-11, but not IL-6, reduces tumor burden in *gp130*^{FF} mice (10, 14). These observations indicate that epithelial tumor promotion can be dependent upon continuous cytokine activation of the GP130/STAT3 signaling cascade.

The mTOR, a serine/threonine kinase that controls cell size and proliferation, is commonly deregulated in human cancers (15). The most common cancer-promoting signaling event that converges on mTOR complex 1 (mTORC1) is aberrant activation of the AKT kinase (16). Increased AKT activity results from unbalanced accumulation of the lipid intermediate phosphoinositol-3-phosphate (PIP_3), an occurrence triggered by excessive activation of the oncogenic phosphoinositide 3-kinase (PI3K) or impaired function of its tumor suppressor counterpart PTEN. Therapeutic inhibition of mTORC1 signaling with analogs of the immunosuppressant rapamycin shows promising results for glioblastoma, breast, endometrial, and renal cell carcinomas (17, 18). Like many other "rapalogs," RAD001 (everolimus) specifically inhibits mTORC1, which promotes protein synthesis, ribosome biogenesis, and cell growth through phosphorylation and activation of the ribosomal p70 S6 kinase (S6K) and the elongation factor 4E-binding protein 4EBP1 (17). Although previous studies suggest an association between inflammatory cytokine abundance and mTORC1 activation (19, 20), the underlying mechanistic links and the significance of inflammation-associated mTORC1 activation during tumorigenesis remain poorly defined.

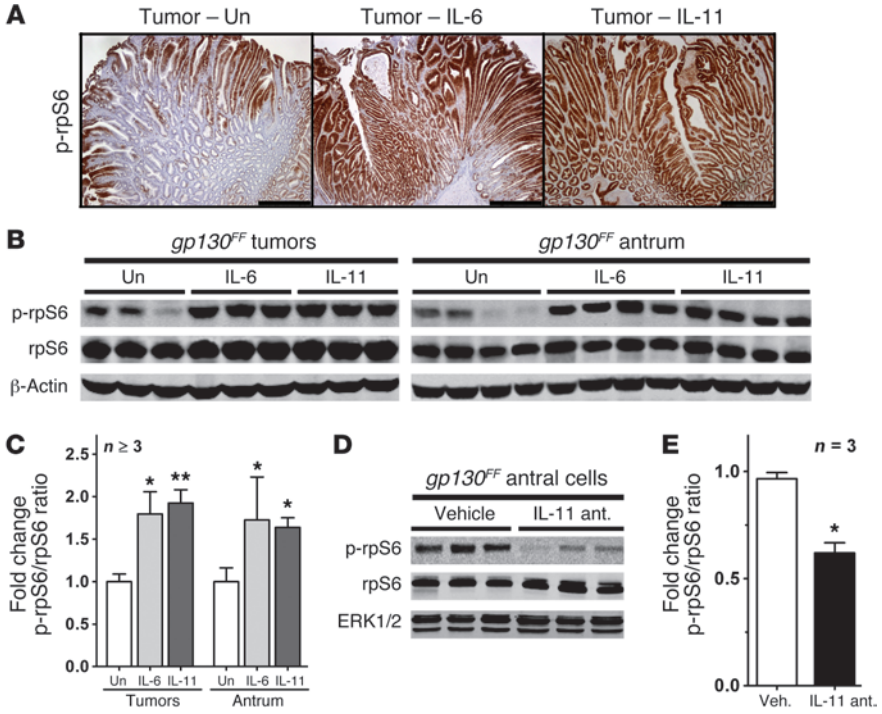

Figure 2
Regulation of mTORC1 activity by GP130 signaling. (**A**) Representative immunostaining for p-rpS6 on sections of gastric tumors from 10-week-old *gp130*^{FF} mice collected 60 minutes after a single i.p. injection of 5 μg of IL-6 or IL-11. Scale bar: 500 μm. (**B** and **D**) Immunoblot analysis (**B**) for p-rpS6 of pooled tumors and unaffected antra from individual mice collected 60 minutes after a single i.p. injection of 5 μg of IL-6 or IL-11 or (**D**) of gastric epithelial cells extracted from the antra of individual mice that have been treated for 4 weeks with an IL-11 antagonist (ant.). Also refer to Supplemental Figure 2. (**C** and **E**) Quantification of the immunoblots shown in (**C**) **B** and (**E**) **D**, expressed as mean fold change ± SEM when compared with the p-rpS6/rpS6 ratio of vehicle-treated (Veh.) mice (**P* < 0.05, ***P* < 0.01). Un, unstimulated.

Here, we reveal an unsuspected driving role for activated mTORC1 signaling in cytokine-dependent tumor promotion. We show that the mTORC1 inhibitor RAD001 affords a surprising therapeutic and prophylactic benefit in 2 gastrointestinal tumor models previously defined by their STAT3 dependency. RAD001 treatment prevented prolonged GP130- and JAK-dependent activation of the PI3K/mTORC1 pathway, without affecting signaling through the prototypical GP130/STAT3 axis. Our results suggest that mTORC1 activation via GP130 is a requirement for inflammation-associated tumorigenesis. Therefore, therapeutic targeting of the druggable PI3K/mTORC1 pathway may be an overlooked Achilles' heel for inflammation-associated malignancies.

Results

Coactivation of mTORC1 and STAT3 in gastric tumors of humans and gp130^{FF} *mice*. To determine the extent of STAT3 and mTORC1 activation in a range of human gastric cancer (GC) subtypes, we used immunohistochemistry to identify the activated (phosphorylated) forms of STAT3 (phosphotyrosine [pY] 705) and the mTORC1 pathway component ribosomal protein S6 (rpS6) (phosphoserine [pS] 240/244). We detected extensive overlap between nuclear pY-STAT3 and cytoplasmic pS-rpS6 staining within the neoplastic epithelium as well as in adjacent stromal and immune cells of all GC biopsies, suggesting frequent coactivation within cells (Figure 1A). Comparison among GC subtypes showed that intestinal-type gastric tumors display the most extensive staining for both pY-STAT3 and pS-rpS6 (Figure 1A and Supplemental Figure 1; supplemental material available online with this article; doi:10.1172/JCI65086DS1). We observed a strikingly similar staining pattern for pY-STAT3 and phosphorylated rpS6 (p-rpS6) in the antra and gastric tumors from *gp130*^{FF} mice, with the most extensive epithelial p-rpS6 staining located toward the luminal edge of tumors (Figure 1B). Furthermore, we observed increased rpS6 and STAT3 phosphorylation in the adjacent, nonadenomatous mucosa of *gp130*^{FF} mice (Figure 1C), suggesting a functional link between STAT3 and mTORC1 signaling irrespective of neoplastic transformation. We speculated that concomitant activation of these pathways may be required to sustain inflammation-associated GC in *gp130*^{FF} mice and humans.

Congruent gene expression signatures between human IGC and tumors in gp130^{FF} *mice*. Intestinal-type GC (IGC) arises most frequently in the glandular epithelium of patients chronically infected with *Helicobacter pylori* and comprises a molecularly and histopathologically distinct type of GC (21), with a prominent proliferative gene signature (22). To determine the molecular subtype of human GC most faithfully replicated by the *gp130*^{FF} model, we first defined a gene expression signature unique to *gp130*^{FF} tumors by comparing tumor tissue to antral stomach tissue from wild-type mice. We identified 324 genes that were upregulated, including the intestine-specific genes *Cdx2*, *Gpa33*, and *Vil1*, and 2,557 genes that were downregulated ($P < 0.05$; Figure 1D and Supplemental Table 1). We then translated this GP130 mouse gene expression signature into an orthologous GP130 human gene expression signature (Supplemental Table 1) to compute a "GP130 activation score" (23) for individual human GC specimens obtained from 2 independent cohorts collected in Singapore ($n = 192$; ref. 24) and Australia ($n = 70$; ref. 22). Strikingly, this analysis revealed that a majority of IGCs had a high GP130 activation score, while most diffuse-type gastric tumors had a low activation score (Figure 1D). Thus, tumors in *gp130*^{FF} mice molecularly and histopathologically (25) recapitulate early stages of human IGC, including metaplastic transformation and excessive mTORC1 and STAT3 activation. Furthermore, the similarity between the *gp130*^{FF} mouse and human IGC gene expression signatures may reflect shared molecular etiology centered on GP130 signaling.

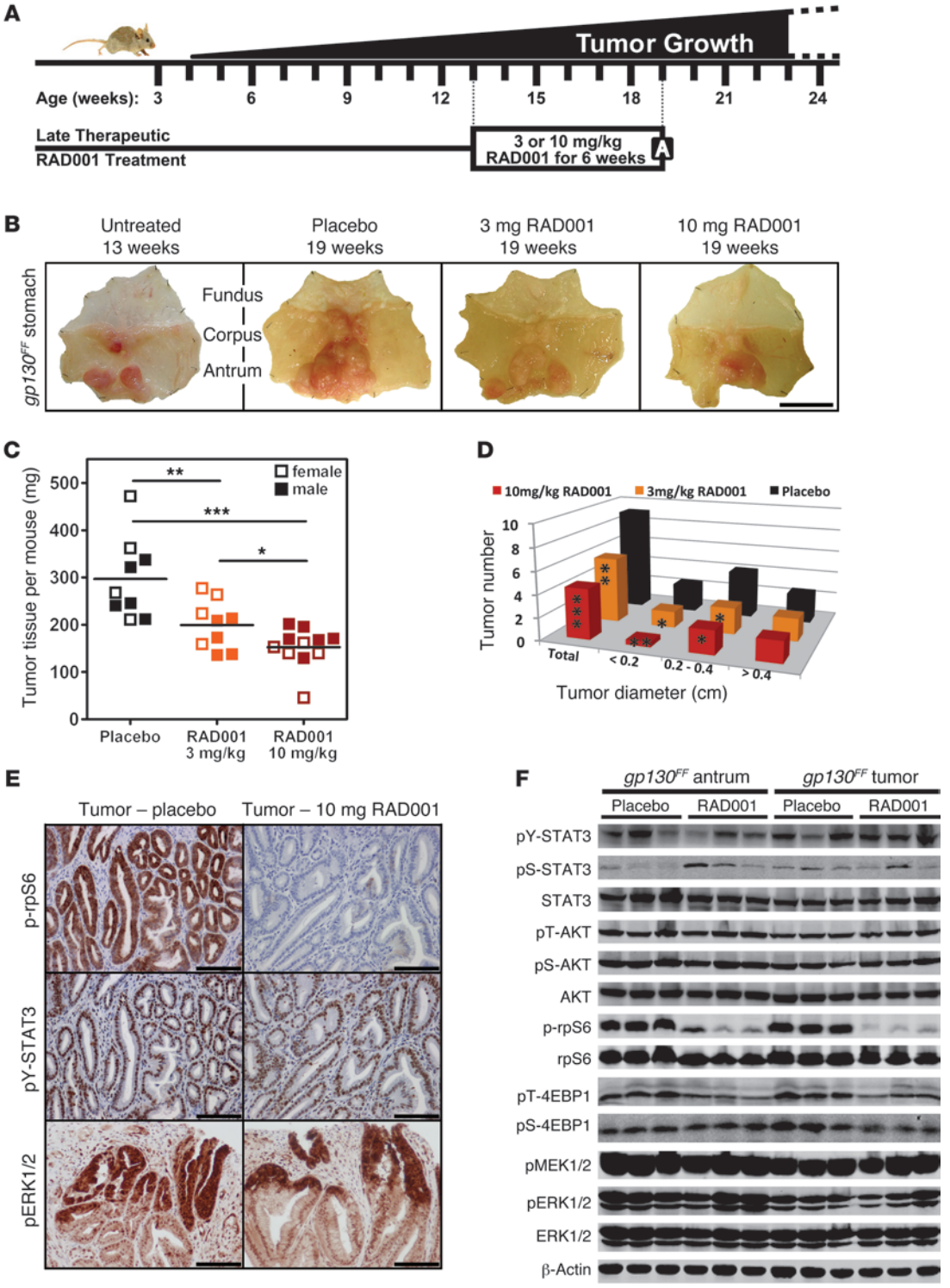

Figure 3
Therapeutic RAD001 treatment of *gp130*^{FF} mice reduces tumor burden. (**A**) Schematic illustration of spontaneous gastric tumorigenesis in *gp130*^{FF} mice and the RAD001 treatment protocol. The boxed "A" indicates the time point of analysis. (**B**) Whole-mount photographs of representative stomachs from *gp130*^{FF} mice at the beginning and end of the RAD001 treatment period. Scale bar: 1 cm. (**C** and **D**) For each individual mouse ($n \geq 9$ per cohort), (**C**) the combined mass of resected tumors was determined and (**D**) individual tumors were enumerated and classified according to their size. Horizontal lines refer to mean values (*$P < 0.05$, **$P < 0.01$, ***$P < 0.001$). Also refer to Supplemental Figures 3 and 4. (**E**) Representative p-rpS6, pY-STAT3, and pERK1/2 immunostainings on tumor sections from RAD001- and placebo-treated *gp130*^{FF} mice. Scale bar: 100 μm. (**F**) Immunoblot analysis of unaffected antra and pooled tumors from individual mice at the end of the RAD001 (10 mg/kg) treatment period. Also refer to Supplemental Figure 5.

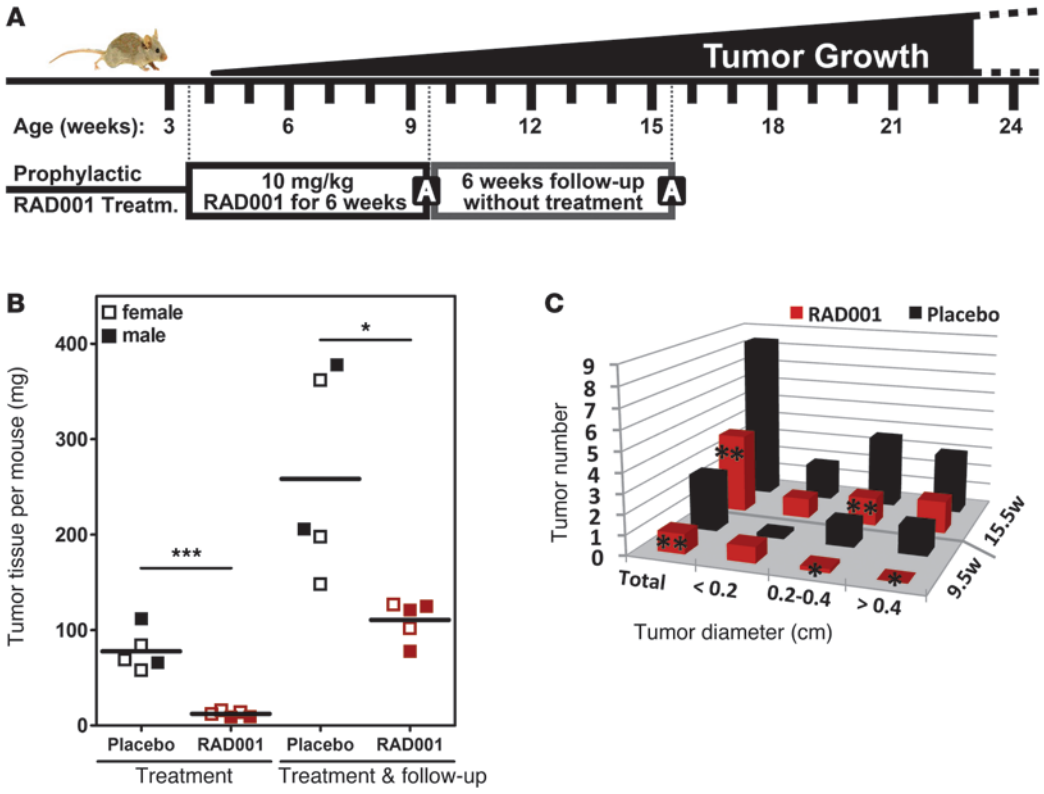

Figure 4

Tumorigenesis in *gp130*^{FF} mice requires continuous mTORC1 activity. (**A**) Twenty-five–day-old (3.5-week-old) *gp130*^{FF} mice were analyzed at the end of the 6-week RAD001 treatment period or after an additional 6-week treatment-free period. (**B** and **C**) For each individual mouse (n = 5 per cohort), (**B**) the combined mass of resected tumors was determined and (**C**) individual tumors were enumerated and classified according to their size. w, weeks. Horizontal lines refer to mean values (*P < 0.05, **P < 0.01, ***P < 0.001). Also refer to Supplemental Figure 6.

Regulation of mTORC1 activity by GP130 signaling. Spontaneous tumor formation in *gp130*^{FF} mice depends on excessive GP130/STAT3 signaling in response to elevated protein levels of IL-11 (10). We therefore investigated whether IL-11 also accounted for mTORC1 activation in *gp130*^{FF} tumors. Indeed, after administration of recombinant IL-11 or IL-6, we detected extensive p-rpS6 staining throughout the epithelial components of the tumors (Figure 2A). Immunoblot analysis revealed a substantial, cytokine-dependent increase of p-rpS6 in both the *gp130*^{FF} tumors and adjacent unaffected antra (Figure 2, B and C). Conversely, p-rpS6 levels were reduced in gastric epithelial cells of *gp130*^{FF} mice therapeutically treated with an IL-11 antagonist (Figure 2, D and E) that was shown to reduce overall tumor burden (14). We have previously observed that tumor promotion in *gp130*^{FF} mice depends on IL-11 rather than IL-6 signaling (10). Concordantly, we found that basal p-rpS6 levels remained elevated in tumors of *gp130*^{FF}*Il6*$^{-/-}$ mice but were reduced in the corresponding unaffected antra of their *gp130*^{FF}*Il11ra*$^{-/-}$ counterparts (Supplemental Figure 2).

Therapeutic RAD001 treatment of gp130^{FF} *mice reduces tumor burden.* Given that mTORC1 activation tracked with gastric tumorigenesis, we hypothesized that pharmacological inhibition of mTORC1 might provide a therapeutic benefit to mice with established tumors. We therefore treated 13-week-old *gp130*^{FF} mice for 6 consecutive weeks with the mTORC1-specific inhibitor RAD001 (Figure 3A). Irrespective of the gender of the mice, RAD001 administration resulted in a dose-dependent reduction in overall tumor mass and primarily reduced the occurrence of smaller tumors (Figure 3, B–D). Accordingly, RAD001 treatment during the early stages of tumorigenesis reduced tumor burden more uniformly in 6-week-old *gp130*^{FF} mice (Supplemental Figure 3, A–D). Hence, mTORC1 activity appears to be required for the growth of emerging gastric lesions rather than for the maintenance of larger established tumors.

Since the ubiquitous expression of the mutant GP130 receptor triggers systemic inflammation in *gp130*^{FF} mice (13), and since IL-6 also induced mTORC1 activity (Figure 2), we next assessed whether RAD001 mediated its therapeutic effect by curbing inflammation. Ablation of *Il6* in *gp130*^{FF} mice ameliorates systemic inflammation, without affecting tumorigenesis (10). Strikingly, RAD001 treatment reduced tumor burden as effectively in *gp130*^{FF}*Il6*$^{-/-}$ mice as in their *Il6*-proficient *gp130*^{FF} counterparts (Supplemental Figure 3, E–G) but had no detectable impact on splenomegaly and thrombocytosis (Supplemental Figure 4), which are associated with STAT3 activation in *gp130*^{FF} mice (10, 26). This suggests that the beneficial effect of RAD001 treatment does not arise from interference with IL-6–mediated systemic inflammation or other effects IL-6 may exert on the neoplastic epithelium.

We then examined whether the therapeutic effect of RAD001 arose through selective inhibition of mTORC1 or indirectly via impairment of STAT3 activation. We found that following RAD001 therapy the phosphorylation levels of STAT3 (pY_{705} and

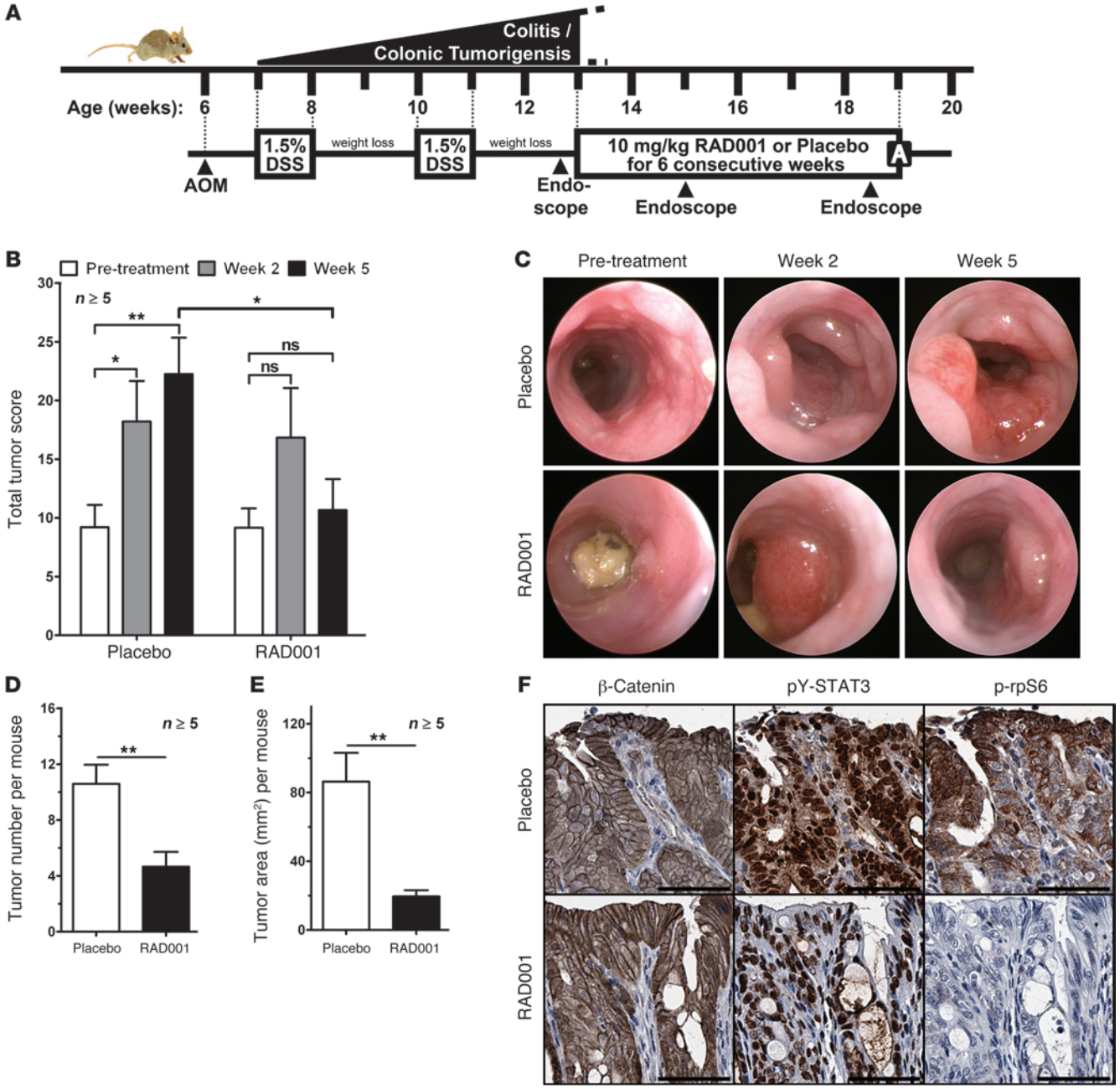

Figure 5

RAD001 suppresses tumor growth in a model of CAC. (**A**) Schematic illustration of colonic tumorigenesis, endoscopy, and the treatment protocol of CAC-challenged wild-type mice. AOM, azoxymethane; DSS, dextran sodium sulphate. (**B**) Tumor burden of individual mice ($n \geq 5$ per cohort) was scored by endoscopy (30) at the indicated time point during RAD001 treatment and is depicted as mean ± SEM (*$P < 0.05$, **$P < 0.01$; ns, not significant). Also refer to Supplemental Figure 7A. (**C**) Representative endoscopy images of the same colonic tumors before and during RAD001 treatment. (**D**) Colon tumor numbers and (**E**) size of individual mice ($n \geq 5$ per cohort) at the end of the RAD001 therapy. Results are mean ± SEM (**$P < 0.01$). Also refer to Supplemental Figure 7B. (**F**) Representative immunostaining for β-catenin, pY-STAT3, and p-rpS6 on colonic tumor sections from RAD001- and placebo-treated mice. Scale bar: 50 μm.

pS_{727}) as well as those of MEK1/2, ERK1/2, and AKT remained unaffected in both the tumors and unaffected antral tissue (Figure 3, E and F). Conversely, phosphorylation of the mTORC1 target rpS6 and, to a lesser extent, 4EBP1 (pS_{64} and phosphothreonine [pT] 36/45) was markedly impaired by RAD001 treatment (Figure 3, E and F). Collectively, these results demonstrate that, even in the presence of excessive STAT3 signaling, tumor promotion in *gp130*^{FF} mice depends on activation of mTORC1.

The activity of mTORC1 is normally constrained by several negative feedback mechanisms. Rapalog treatment has been shown

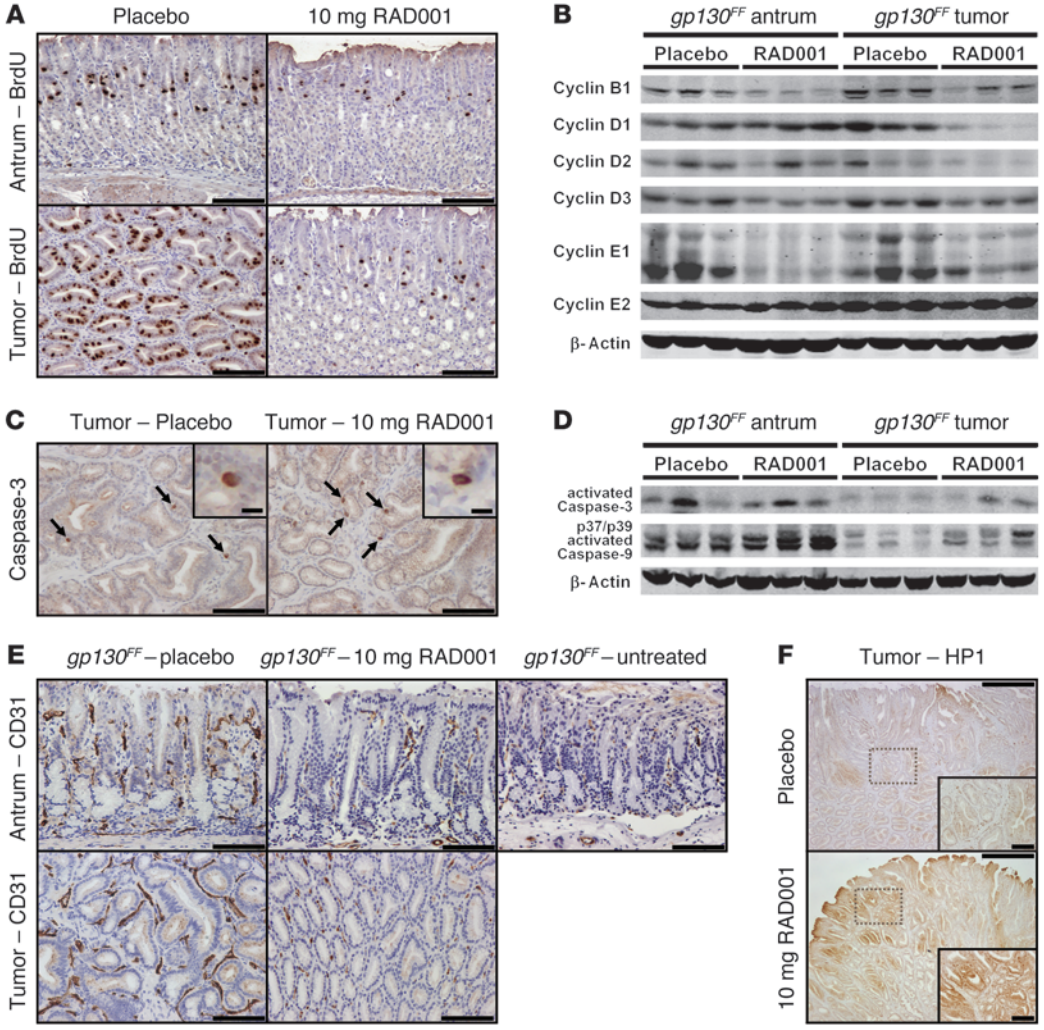

Figure 6

RAD001 treatment decreases tumor cell proliferation and induces tissue hypoxia. (**A**, **C**, **E**, and **F**) Representative immunostaining for (**A**) BrdU, (**C**) active caspase-3, (**E**) CD31, and (**F**) hypoxyprobe-1 (HP1) on sections of unaffected antra and tumors from 19-week-old *gp130*^{FF} mice collected after 6 weeks of RAD001 (10 mg/kg) treatment. (**C**) Apoptotic cells are indicated by arrows. Scale bar: 10 μm (insets in **C**); 100 μm (**A**, **C**, **E**, and insets in **F**); 500 μm (**F**). Also refer to Supplemental Figure 8. (**B** and **D**) Immunoblot analysis of unaffected antra and pooled tumors from individual 19-week-old *gp130*^{FF} mice collected after 6 weeks of RAD001 (10 mg/kg) treatment.

to disrupt this feedback, leading to derepression of the upstream PI3K/AKT pathway and limiting the efficacy of rapalogs in the clinic (27). However, we did not detect an increase in pS-AKT and pT-AKT (Figure 3F) or in phosphorylation of the AKT substrates Bad and Pras40 (Supplemental Figure 5A) after treating *gp130*^{FF} mice for 6 consecutive weeks with RAD001. Similar results were observed after shorter RAD001 treatment periods (Supplemental Figure 5B), suggesting that feedback activation of PI3K/AKT does not occur in *gp130*^{FF} mice. This could be reconciled with downregulation of expression of insulin-like growth factor receptor 1 (*Igfr1*), a receptor important for IGF-mediated activation of the PI3K pathway (28), in RAD001-treated mice (Supplemental Figure 5C).

Formation and development of gp130^{FF} *tumors requires continuous mTORC1 activity*. To further explore whether mTORC1 signaling was required for de novo tumor formation, we treated tumor-free 3.5-week-old *gp130*^{FF} mice prophylactically with RAD001 (Figure 4A). RAD001 administration almost completely abolished tumor formation, with the occasional tumor that formed remaining very small (Supplemental Figure 6A). This prophylactic effect was dependent on continuous mTORC1 restriction, as termination of RAD001 treatment coincided with the emergence of new tumors (Figure 4, B and C, and Supplemental Figure 6A) and the re-appearance of epithelial p-rpS6 staining (Supplemental Figure 6B). These observations indicate that suppression of mTORC1 activity was not sustained during the RAD001-free follow-up period. Collectively, our results suggest that continuous mTORC1 activity is a requirement for the initiation and development of inflammation-dependent gastric tumors.

RAD001 suppresses tumor growth in colitis-associated cancer in wild-type mice. To establish whether the therapeutic benefits conferred by RAD001 extended to other inflammation-associated cancer models, we induced colitis-associated cancer (CAC) in wild-type mice (Figure 5A). In this model, tumorigenesis is initiated through mutagen-induced activation of the canonical Wnt/β-catenin path-

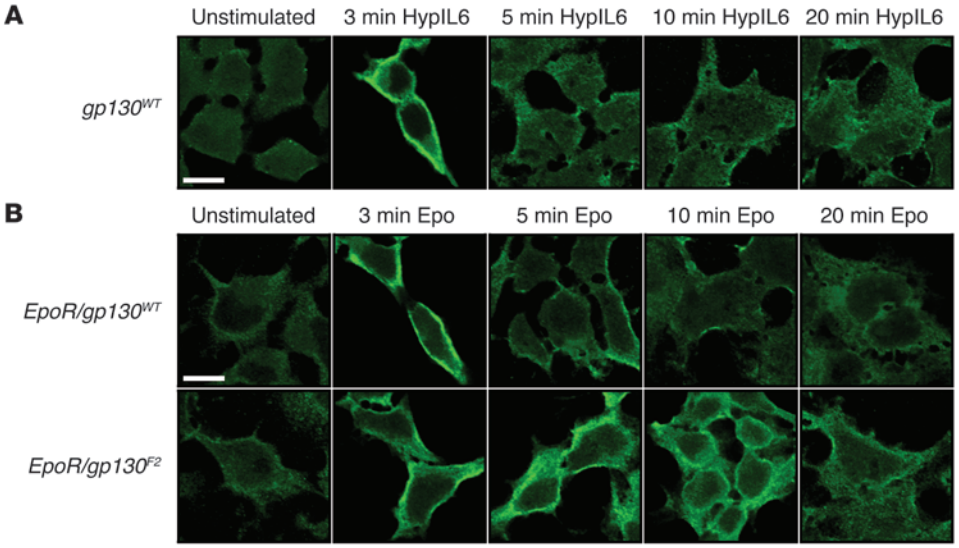
A
Unstimulated
3 min HypIL6
5 min HypIL6
10 min HypIL6
20 min HypIL6
gp130WT
B
Unstimulated
3 min Epo
5 min Epo
10 min Epo
20 min Epo
EpoR/gp130WT
EpoR/gp130F2

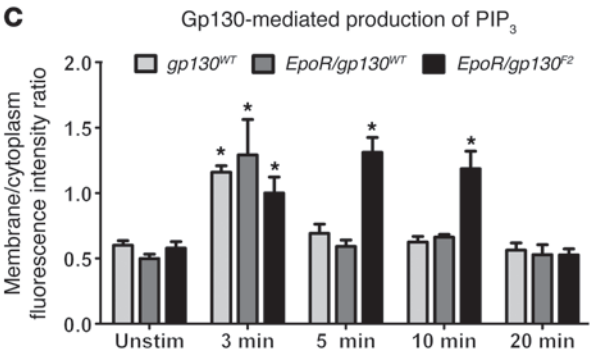
C
Gp130-mediated production of PIP3
gp130WT
EpoR/gp130WT
EpoR/gp130F2
Membrane/cytoplasm fluorescence intensity ratio
2.0
1.5
1.0
0.5
0.0
Unstim
3 min
5 min
10 min
20 min

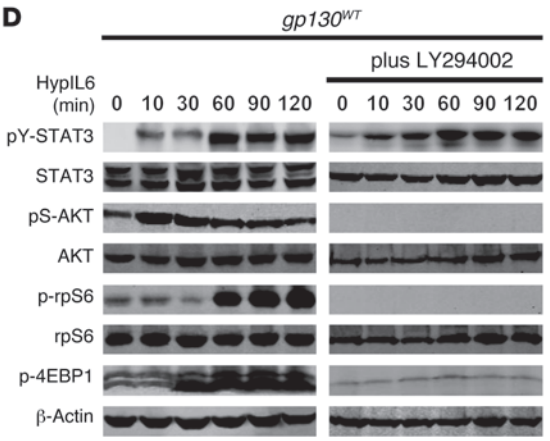
D
gp130WT
plus LY294002
HypIL6 (min)
0 10 30 60 90 120
0 10 30 60 90 120
pY-STAT3
STAT3
pS-AKT
AKT
p-rpS6
rpS6
p-4EBP1
β-Actin

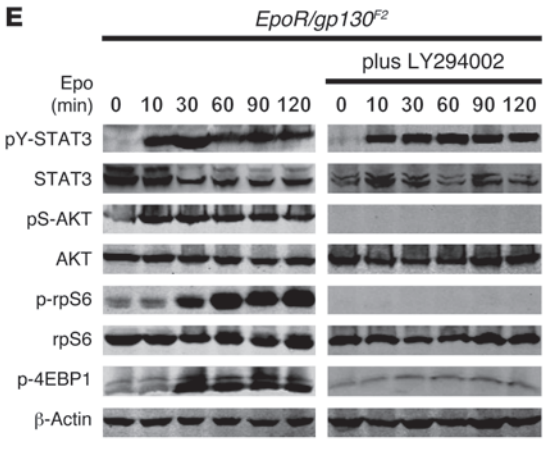
E
EpoR/gp130F2
plus LY294002
Epo (min)
0 10 30 60 90 120
0 10 30 60 90 120
pY-STAT3
STAT3
pS-AKT
AKT
p-rpS6
rpS6
p-4EBP1
β-Actin

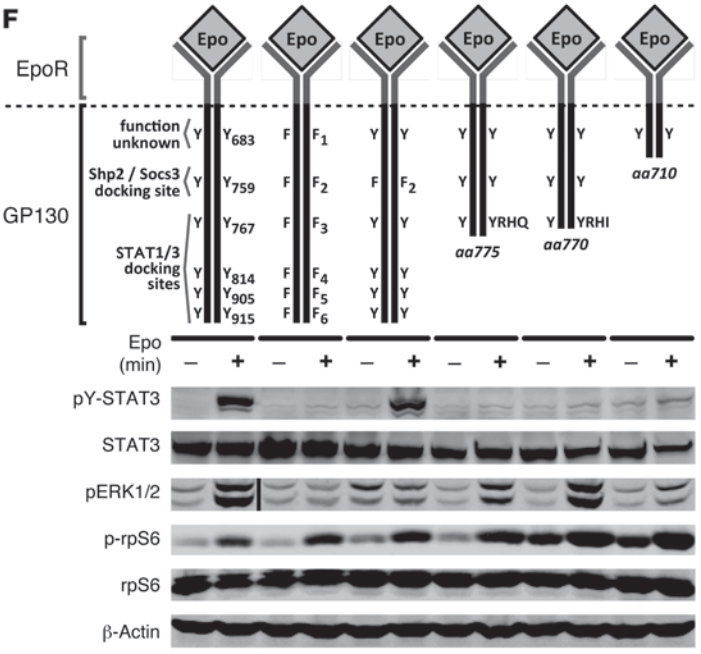
F
Epo
EpoR
GP130
function unknown
Shp2 / Socs3 docking site
STAT1/3 docking sites
Y683
Y759
Y767
Y814
Y905
Y915
F1
F2
F3
F4
F5
F6
YRHQ
YRHI
aa775
aa770
aa710
Epo (min)
– + – + – + – + – + – +
pY-STAT3
STAT3
pERK1/2
p-rpS6
rpS6
β-Actin

Figure 7
Excessive PIP_3 accumulation and mTORC1 activation in cells expressing mutant GP130. (**A**–**C**) Formation of PIP_3 at the cell membrane was monitored as an indicator of PI3K activity by immunofluorescent staining using the PIP_3-specific GST-GRP1PH probe. The representative images show (**A**) naive 293T cells or (**B**) cells transiently expressing the indicated chimeric EpoR/GP130 receptor. Cells were stimulated for the indicated time with hyper–IL-6 (HypIL6; 100 ng/ml) or Epo (50 U/ml). (**C**) Images were then used for cell segmentation analysis and quantification with MetaMorph software. For each time point a total of 150 to 300 cells was analyzed, and results are depicted as mean ± SEM (*P < 0.05 when compared with unstimulated isogenic cells). Scale bar: 10 μm. Also refer to Supplemental Figure 9. (**D** and **E**) Immunoblot analysis of (**D**) naive 293T cells or (**E**) cells transiently expressing the *EpoR/gp130^{F2}* receptor. Cultures were serum starved and, where indicated, exposed to the PI3K inhibitor LY294002 (25 μM) 60 minutes prior to stimulation with hyper–IL-6 (100 ng/ml) or Epo (50 U/ml) for the indicated period. (**F**) Immunoblot analysis of 293T cells transiently expressing the indicated mutant EpoR/GP130 receptor. Serum-starved cells were stimulated for 60 minutes with Epo (50 U/ml). The schematic shows the transfected EpoR/GP130 receptors, which encode tyrosine (Y) to phenylalanine (F) substitution or truncation mutations in the cytosolic domain of human GP130. The consensus function of the individual Y residues and their amino acid position are depicted. Also refer to Supplemental Figure 11. Note that the pERK1/2 lanes were run on the same gel but were noncontiguous.

way, while colitis-associated inflammation promotes survival and proliferation of neoplastic epithelial cells via GP130/STAT3 activation (29). We used endoscopy to monitor colonic tumor burden over time and generate corresponding tumor scores (30). RAD001 therapy stabilized or decreased colonic tumor burden over the 6-week treatment period, whereas tumor burden in all mice of the placebo-treated cohort invariably increased (Figure 5B and Supplemental Figure 7A). Furthermore, endoscopy revealed a RAD001-dependent reduction in the size of individual colonic tumors (Figure 5C). At autopsy, RAD001-treated mice showed a significant reduction in the overall tumor number and total tumor area compared with those of placebo-treated controls (Figure 5, D and E, and Supplemental Figure 7B). In placebo-treated mice, we confirmed prominent nuclear pY-STAT3 staining in the neoplastic epithelium and in tumor-adjacent stromal and immune cells and also found extensive rpS6 phosphorylation at the luminal edges of colonic tumors (Figure 5F). Consistent with our observations in gastric tumors of *gp130^{FF}* mice, RAD001 treatment almost completely abolished p-rpS6, but not pY-STAT3, staining in colonic tumors (Figure 5F). By contrast, RAD001 did not alter the epithelial β-catenin staining pattern, suggesting that its therapeutic effect was not mediated through interference with the aberrantly activated Wnt pathway (31). These findings illustrate that mTORC1 restriction also impairs inflammation-associated colonic tumorigenesis fueled by excessive GP130/STAT3 activation in wild-type mice. Collectively, the observed efficacy of RAD001 in both the *gp130^{FF}* and CAC models suggests that GP130-mediated mTORC1 activation may commonly contribute to inflammation-associated tumor promotion.

RAD001 treatment decreases tumor cell proliferation and induces tissue hypoxia. To elucidate the mechanisms by which RAD001 decreased inflammation-associated tumor burden, we assessed cell proliferation in the gastric epithelium of *gp130^{FF}* mice by bromodeoxyuridine (BrdU) incorporation. We detected a marked reduction in the number of BrdU-positive cells in unaffected antral and tumor tissue of RAD001-treated mice (Figure 6A and Supplemental Figure 8A). Reduced proliferation coincided with decreased expression of the cell-cycle regulators cyclin B1, D1, D2, D3, and E1 within the tumors as well as cyclin B1, D3 and E1 in the unaffected antra (Figure 6B). In contrast, RAD001 treatment did not alter the frequency of tumor cell apoptosis, as detected using the apoptotic markers cleaved caspase-3 and caspase-9 and TUNEL staining (Figure 6, C and D, and data not shown). However, staining for the endothelial cell marker CD31 revealed a significant reduction in blood vessel density in the tumors and unaffected antra of RAD001-treated *gp130^{FF}* mice (Figure 6E and Supplemental Figure 8B). This coincided with reduced expression of angiopoietin 2 (*Angpt2*) (Supplemental Figure 8D), which is typically produced by endothelial cells during tumor vascularization (32, 33). Consistently, immunostaining for hydroxyprobe-1 suggested elevated levels of tissue hypoxia in RAD001-treated *gp130^{FF}* tumors (Figure 6F and Supplemental Figure 8C). However, as previously reported (34), RAD001 treatment prevented induction of hypoxia-inducible factor 1α (*Hif1a*) at both the transcript and protein level (Supplemental Figure 8, D and E). Expression of *Vegfa*, a transcriptional target for Hif1α as well as STAT3 (35), also remained unchanged following RAD001 treatment (Supplemental Figure 8, D–F).

GP130 activates mTORC1 via PI3K/AKT in a STAT3- and STAT1-independent manner. To explore whether GP130 stimulates the mTORC1 pathway through PI3K activation, we monitored subcellular relocalization of the PI3K product PIP_3, using a glutathione-*S*-transferase–tagged (GST-tagged) pleckstrin homology domain from the phosphoinositides-1 receptor GRP1 as a probe (36). Compared with the diffuse background staining observed in unstimulated 293T cells, exposure to the designer cytokine hyper–IL-6 (human IL-6 fused to its α-receptor; ref. 37) resulted in transient accumulation of PIP_3 at the plasma membrane within 3 minutes (Figure 7A). We observed similar kinetics of PIP_3 accumulation after erythropoietin (Epo) stimulation of cells transfected with a chimeric receptor comprising the extracellular domain of the Epo receptor fused to the intracellular domain of human wild-type GP130 (*EpoR/gp130^{WT}*; Figure 7, B and C). By contrast, stimulation of the *EpoR/gp130^{F2}* mutant, which encodes the human equivalent (gp130^{Y759F}) of the murine gp130^{Y757F} substitution (12), triggered excessive and prolonged PIP_3 accumulation at the plasma membrane (Figure 7, B and C), while untransfected 293T cells did not respond to Epo (Supplemental Figure 9A). Immunoblot analyses revealed that stimulation of both the endogenous and chimeric GP130 receptors resulted in PI3K-dependent phosphorylation of AKT and the mTORC1 substrates rpS6 and 4EBP1, which was prevented in cells pretreated with the PI3K inhibitor LY294002 (Figure 7, D and E).

To confirm that PI3K activation was STAT3 independent, we interfered with endogenous STAT3 activity in 293T cells using either STAT3 siRNA or a dominant-negative variant of STAT3. Effective STAT3 suppression was confirmed by immunoblot and by measuring the activity of a STAT3-responsive luciferase reporter construct (*APRE-Luc*; Supplemental Figure 9, B and C). Importantly, STAT3 inhibition did not affect subcellular relocalization of PIP_3 in cells harboring either the wild-type or the *EpoR/gp130^{F2}* receptor (Supplemental Figure 9, D–I). Furthermore, PIP_3 accumulation remained prolonged following stimulation of the *EpoR/gp130^{F2}* receptor (Supplemental Figure 9, G–I). Similarly, we found that administration of recombinant IL-11 or IL-6 consistently induced p-rpS6 in the antra of *gp130^{FF}Stat3$^{+/-}$* mice as well as in the tumors and antra of *gp130^{FF}Stat1$^{-/-}$* mice

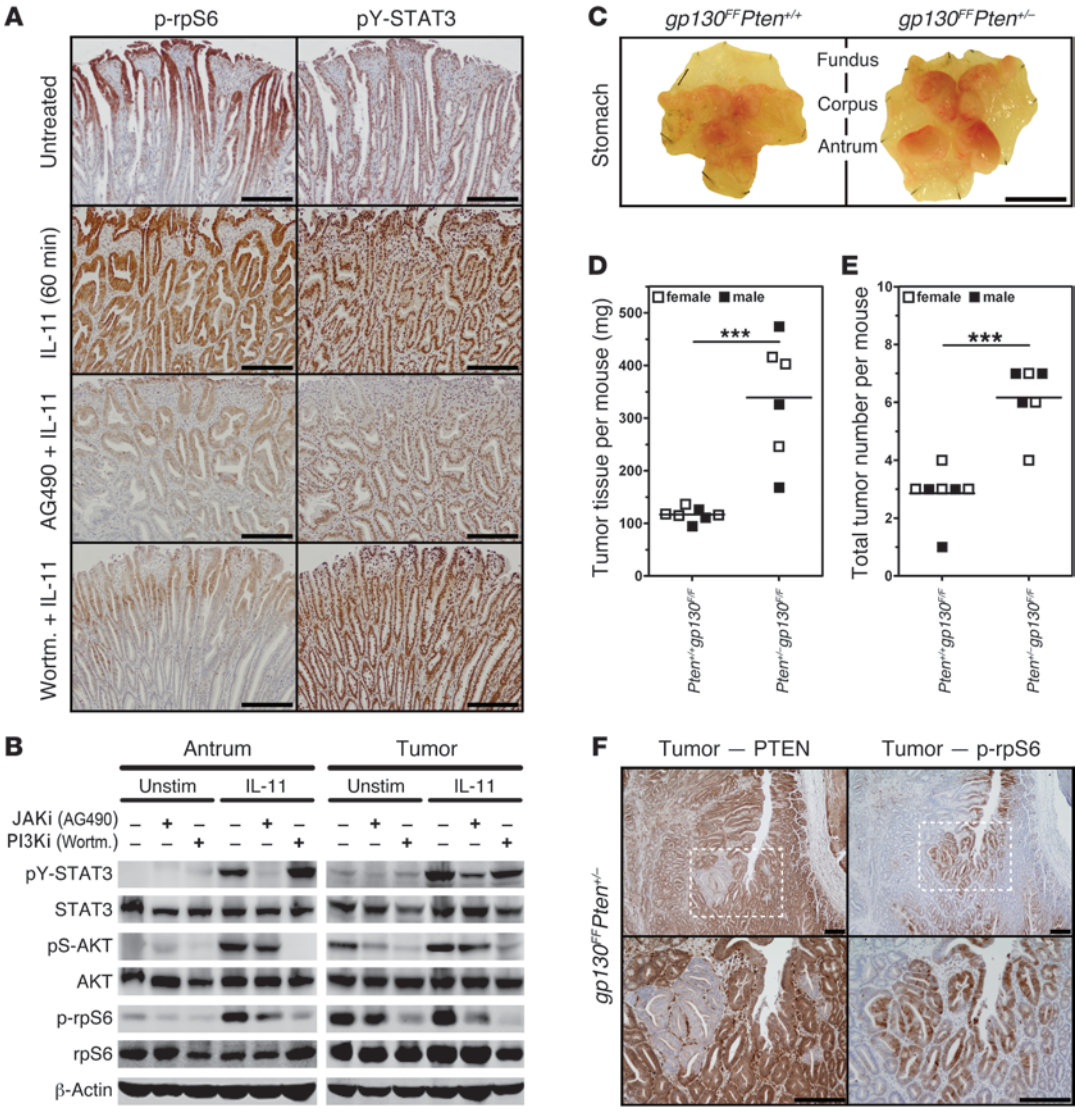

Figure 8

Activation of PI3K/mTORC1 via GP130 is JAK dependent and cooperates with impaired PTEN activity. (**A**) Representative immunostaining for p-rpS6 and pY-STAT3 on sections of gastric tumors from 10-week-old *gp130^{FF}* mice collected 60 minutes after a single i.p. injection of 5 μg IL-11. Where indicated, mice were treated with a JAK (AG490) or PI3K (wortmannin [Wortm]) inhibitor 45 minutes prior to stimulation. Scale bar: 200 μm. (**B**) Immunoblot analysis of unaffected antra and pooled tumors from individual 10-week-old *gp130^{FF}* mice collected 60 minutes after a single i.p. injection of 5 μg IL-11. Where indicated, mice were treated with the pan-JAK inhibitor (JAKi) AG490 (40 mg/kg) or the PI3K inhibitor (PI3Ki) wortmannin (5 mg/kg) 45 minutes prior to IL-11 administration. Also refer to Supplemental Figure 11C. (**C**) Whole-mount photographs of representative stomachs from 14-week-old mice with the indicated genotype. Scale bar: 1 cm. (**D** and **E**) For each individual mouse ($n \geq 6$ per cohort), (**D**) the combined mass of resected tumors was determined and (**E**) individual tumors were enumerated. Horizontal lines refer to mean values (***$P < 0.001$). (**F**) Representative PTEN and p-rpS6 immunostaining on adjacent tumor sections from 14-week-old *gp130^{FF}Pten$^{+/-}$* mice. The bottom panel shows the boxed regions at in higher magnification. Scale bar: 200 μm.

(Supplemental Figure 10). Collectively, these results suggest that GP130-dependent PI3K/mTORC1 activation occurs independently of STAT3 and STAT1.

PI3K/mTORC1 pathway activation requires JAK activity but not GP130 tyrosine phosphorylation. Activation of PI3K is frequently preceded by binding of the SH2 domain within the regulatory p85 subunits to phosphorylated tyrosine residues on receptors (38). We therefore monitored Epo-dependent rpS6 activation in 293T cells that expressed chimeric EpoR/GP130 receptor constructs harboring a series of tyrosine-to-phenylalanine substitutions. We detected robust p-rpS6 induction in the absence of individual tyrosine residues (data not shown) and also in the absence of all functional GP130 tyrosine residues (Figure 7F). In addition, GP130 receptors with truncation mutations distal to the Box1/2 homology region, which is required for constitutive association between GP130 and JAK family kinases (8), also triggered rpS6 phosphorylation (Figure 7F). We confirmed our findings in the unrelated BaF3 cell line, which stably expresses the human

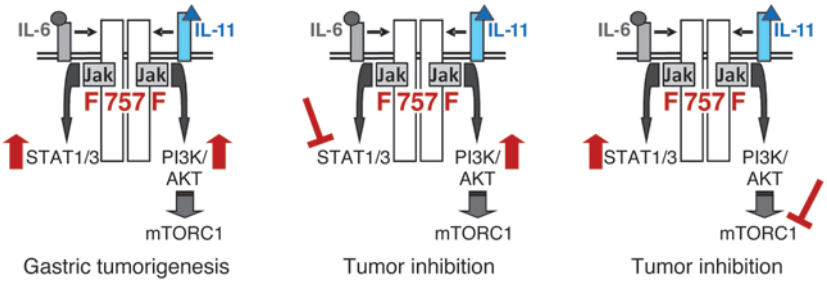

Figure 9
Gp130-dependent simultaneous activation of PI3K/mTORC1 and STAT3 facilitates tumor promotion. Schematic representation of GP130/JAK-dependent intracellular signaling in the neoplastic gastric epithelium of *gp130*^{FF} mice, which triggers parallel and excessive coactivation (↑) of STAT3 and PI3K/mTORC1. (**A**) Simultaneous activation of both pathways is required for the promotion and maintenance of gastric tumors, and (**B** and **C**) pharmacological inhibition of either cascade impairs tumor growth.

IL-11Rα to permit IL-11–mediated GP130 activation. Stimulation of endogenous GP130 by IL-11 as well as of mutant EpoR/GP130 receptors resulted in transient AKT phosphorylation and robust activation of rpS6, even in the absence of all GP130 tyrosine residues (Supplemental Figure 11, A and B).

To clarify the hierarchy between IL-11–dependent STAT3 and PI3K activation, we pretreated IL-11Rα–expressing BaF3 cells with either the PI3K inhibitor LY294002 or the pan-JAK inhibitor AG490. Treatment with AG490 revealed that JAK activity was not only required for STAT3 activation but also for IL-11–dependent AKT and rpS6 phosphorylation (Supplemental Figure 11C). By contrast, LY294002 completely prevented AKT and rpS6 phosphorylation without affecting STAT3 activation. Similarly, pretreatment of *gp130*^{FF} mice with AG490 inhibited IL-11–mediated AKT, rpS6, and STAT3 phosphorylation in the antra and gastric tumors, while the same challenge in wortmannin-treated *gp130*^{FF} mice only suppressed AKT and rpS6 activation (Figure 8, A and B). Notwithstanding the imperfect selectivity of the above inhibitors (39), our results suggest that IL-11–dependent engagement of the PI3K/mTORC1 pathway occurs independently of GP130 tyrosine phosphorylation but requires activation of (GP130-associated) JAK kinases.

Synergistic interaction between GP130 and PI3K signaling exacerbates gastric tumorigenesis. Having established that PI3K pathway activation is required for gastric tumor formation in *gp130*^{FF} mice, we hypothesized that a PI3K pathway "activation signature" may also be evident in inflammation-associated GCs in humans. We derived a PI3K activation gene signature for human mammary epithelial cells transduced with the p110α isoform of PI3K (ref. 40, Supplemental Figure 12A, and Supplemental Table 2). This PI3K expression profile was used to compute a "PI3K activation score" for individual human cancers of our GC data sets (see Figure 1D). Strikingly, we found that a majority of IGCs had a high PI3K activation score, while most diffuse-type gastric tumors had a low activation score (Supplemental Figure 12B), indicating that PI3K pathway activation is a common molecular feature of IGC.

Early stages of sporadic GC are associated with impaired PTEN activity (17, 41), and loss of *PTEN* heterozygosity in patients with the inherited Cowden syndrome promotes the growth of hyperplastic intestinal polyps (42). To explore whether further deregulation of PI3K/mTORC1 pathway activity would exacerbate GP130-driven gastric tumorigenesis, we generated *gp130*^{FF}*Pten*$^{+/-}$ compound mutant mice. As expected, we observed an increase in gastric tumor burden in these mice when compared with their *Pten*-proficient counterparts (Figure 8, C–E). Immunohistochemical analysis of tumor sections highlighted a striking correlation between areas of excessive rpS6 phosphorylation and complete loss of PTEN staining (Figure 8F), indicative of spontaneous loss of heterozygosity. Furthermore, we have observed that selective *Pten* ablation in the neoplastic gastric epithelium also increased tumor burden in corresponding *gp130*^{FF}*Pten*$^{fl/fl}$ compound mutant mice (M. Buchert and M. Ernst, unpublished observations). These observations indicate that GP130-independent PI3K/mTORC1 pathway activation synergizes with aberrant GP130 activity to drive tumor development.

Collectively, our results presented here demonstrate that engagement of the shared GP130 receptor by IL-6 family cytokines simultaneously activates the STAT3 and PI3K/mTORC1 pathways within neoplastic cells to synergistically facilitate inflammation-associated tumor promotion (Figure 9).

Discussion

It is now widely accepted that chronic inflammation and inflammation-like conditions within the cytokine-rich tumor microenvironment contribute to cancer development. One molecular hallmark of inflammation-associated tumors is aberrant activation of epithelial STAT3, which acts as a master regulator of proliferation, survival, and angiogenesis programs in growing tumors (1, 7). Constitutive activation of the GP130/JAK/STAT3 pathway in humans has been associated with somatic gain-of-function mutations in *GP130* or *STAT3* in hepatocellular carcinomas (43, 44), *JAK1* in acute leukemia and some solid cancers (45), and *JAK2* in myeloproliferative neoplasms (46) as well as in response to epigenetic silencing of the negative regulator *SOCS3* in lung cancers (47). However, aberrant STAT3 activity is most frequently observed in tumors where pathway-activating mutations are not detectable, suggesting a prevalent paracrine mode of STAT3 activation.

IL-6 family cytokines are abundant in inflammation-associated tumor settings and are produced by tumor-infiltrating monocytes/macrophages and stromal cells as well as the neoplastic cells themselves (1, 10). The importance of paracrine GP130/JAK/STAT3 pathway activation by these cytokines is evident in several inflammation-associated tumorigenesis models. For example, tumor promotion in the murine CAC model relies on myeloid cell–derived cytokines (48) and is highly sensitive to genetic and

pharmacological restriction of IL-6 and IL-11 activity (29, 49). A similar cytokine involvement has also been proposed for IL-6 in hepatocellular carcinoma (50), renal cell carcinoma, and prostate cancer (51) and for IL-11 in gastric tumorigenesis in *gp130^{FF}* mice (10). Hence, IL-6 family cytokines fuel tumor development in a range of epithelial malignancies.

Here, we pursued preliminary evidence linking mTORC1 signaling to inflammation and tumor promotion (19, 20). Our analysis indicated that phosphorylation of rpS6, a downstream target of mTORC1, commonly occurs alongside STAT3 activation in human GC. In the *gp130^{FF}* mouse model of IGC, we linked coactivation of mTORC1 and STAT3 within tumor cells to GP130 ligation by IL-6 family cytokines. To determine whether mTORC1 activation was a driver of inflammation-associated tumor development, we used the mTORC1-specific inhibitor RAD001 in 2 genetically distinct inflammation-associated tumor models, namely CAC in wild-type mice and IGC in *gp130^{FF}* mice. In both settings, RAD001 effectively suppressed tumor development. RAD001 therapy reduced cell proliferation, cyclin expression, and vascularization of established gastric tumors and thus also prevented the emergence of nascent tumors in *gp130^{FF}* mice.

The effect of RAD001 in our murine tumor models is broadly consistent with clinical trial data, which show that RAD001 as a single agent exerts a modest therapeutic benefit in patients with advanced, chemotherapy-resistant GC (refs. 41, 52, 53; GRANITE-1 Phase III Study) or colorectal cancer (ref. 54; Phase II Study). Predictably, however, the efficacy of RAD001 in our early-stage gastric and colorectal cancer models was greater than that in these unstratified cohorts of patients with advanced disease. Nevertheless, consistent between our observations and clinical studies, the predominant mode of action of RAD001 was cytostatic rather than proapoptotic (18, 41, 52). Consequently, ongoing RAD001 administration was required to maintain tumor cytostasis in *gp130^{FF}* mice. Surprisingly, even after 6 consecutive weeks of RAD001 therapy, we did not detect RAD001-induced feedback activation of the PI3K/AKT pathway (i.e., increased AKT phosphorylation or activity) that has been described in human cancers and which is thought to contribute to drug resistance (27, 28). This suggests that PI3K/AKT derepression does not occur in RAD001-treated *gp130^{FF}* mice.

In order to verify the involvement of the PI3K/mTORC1 pathway in our tumor models, we treated *gp130^{FF}* mice with the dual PI3K and mTOR inhibitor BEZ235 (Novartis). BEZ235 exerted a cytostatic effect similar to that of RAD001, despite dual inhibition of both AKT and rpS6 phosphorylation (S. Thiem and M. Ernst, unpublished observations). Therefore, we believe that the cytostatic effects of RAD001 were unlikely to be mediated by off-target activity. These results are consistent with emerging evidence that targeting the PI3K/mTORC1 pathway in isolation reduces cell proliferation but typically remains insufficient to induce tumor cell apoptosis, partly due to induction of cellular stress-like responses and upregulation of antiapoptotic proteins such as Bcl-2 and Bcl-X (55). Accordingly, we have found that RAD001 administration reduces tumor burden more effectively in *gp130^{FF}Bcl2$^{+/-}$* compound mutant mice than in *gp130^{FF}* mice (S. Thiem and M. Ernst, unpublished observations). Therefore, targeting these cooperative cell growth and survival networks with multiple inhibitors may be required for tumor-specific cytotoxicity.

While activation of the PI3K pathway by IL-6 family cytokines has previously been observed, the underlying molecular mechanism has remained controversial. We performed a functional assessment of the GP130 receptor in cell lines to clarify the molecular link between GP130 engagement and mTORC1 activation. Previous studies suggested an involvement of the phosphorylated gp130^{Y2} (i.e., murine gp130^{Y757}) residue and the associated SHP1/2 proteins (56) or binding of PI3K to activated STAT3 (57). Contrary to these reports, our data provide compelling genetic evidence for a STAT3- and gp130^{Y2} residue/SHP2-independent mechanism. We also found that STAT3 phosphorylation remained unaffected in *gp130^{FF}* mice after RAD001 treatment, contravening suggestions that mTORC1 can directly promote serine, and indirectly tyrosine, phosphorylation of STAT3 (20, 58). Our data indicate that, downstream of GP130, activation of STAT3 and mTORC1 occurs independently (Figure 9). Furthermore, both JAK and PI3K inhibitors attenuated GP130-mediated mTORC1 activation in vitro and in vivo, implying that signal transduction occurs via JAK-mediated activation of the PI3K/AKT/mTORC1 signaling axis. This signal transduction model is consistent with findings that the p85 subunit of PI3K can directly (and indirectly) associate with activated JAK kinases (59, 60). Downstream of mTORC1, we observed that RAD001 treatment predominantly abrogated phosphorylation of rpS6 but had a less dramatic effect on 4EBP1 phosphorylation. This inhibition profile is typical for rapalogs (55) and suggests that the therapeutic effect of RAD001 in *gp130^{FF}* mice is related to suppression of S6K and rpS6, rather than suppression of 4EBP1. Collectively, our results clarify the mechanism by which IL-6 family cytokines activate the PI3K/mTORC1 pathway, a molecular link that may fuel tumor promotion in a range of inflammation-associated malignancies.

The ability of IL-6 family cytokines to activate PI3K through GP130 reveals what we believe to be a novel mechanism of protumorigenic PI3K/AKT/mTORC1 pathway activation. Excessive mTORC1 activity is commonly observed in human cancers harboring mutations that activate the PI3K pathway (16, 17, 61). Our data illustrate that tumor-promoting PI3K/mTORC1 signaling can also result from potentiating events in the upstream GP130/JAK cascade, as modeled in *gp130^{FF}* mice and corresponding gp130^{F2} cells. Cytokine stimulation of this hypermorphic mutant receptor led to sustained and exaggerated mTORC1/S6K activation that, in conjunction with STAT3, is required for gastric tumor promotion in *gp130^{FF}* mice. With respect to the signaling outcomes, *gp130^{FF}* mice and gp130^{F2} cells have substantial molecular parallels, with tumors driven by inactivation of *SOCS3*, GP130/JAK-activating mutations, or abundant cytokines within the inflamed tumor microenvironment. Indeed, the striking congruence of gene expression patterns between *gp130^{FF}* adenomas and human IGC specimens suggests that aberrant GP130 signaling may be central to both murine and human diseases. Significantly, we observed that GP130-mediated mTORC1 activation also occurred downstream of the unmutated GP130 receptor in vitro and in vivo, demonstrating that this molecular link is not restricted to *gp130^{FF}* mice and gp130^{F2} mutant cells. The efficacy of RAD001 in the CAC setting suggests that cytokine activation of the wild-type GP130/PI3K/mTORC1 axis also supports inflammation-associated tumor development. Based on these findings, we propose that inhibitors of GP130/PI3K/mTORC1 signaling are readily testable therapeutic options for inflammation-associated malignancies in humans.

Characterizing the degree of PI3K/mTORC1 pathway activation in different GC subtypes, as well as their sensitivity to PI3K/mTORC1 inhibitors, is likely to facilitate effective stratification of treatments in the clinic. Our subtype-specific

immunohistochemistry analysis demonstrates that the PI3K/mTORC1 and STAT3 pathways are commonly coactivated in each of the GC subtypes assessed. However, the IGC subtype exhibited the most extensive activation of both pathways, and its gene expression profile was most similar to the PI3K activation gene signature. The efficacy of RAD001 in our murine IGC model therefore suggests that patients with IGC may show the most profound response to PI3K/mTOR inhibitors. Nevertheless, the possibility that PI3K pathway activation is important for the genesis of other GC subtypes cannot be excluded. To define the importance of PI3K/AKT/mTORC1 activation across the spectrum of GC subtypes, the functional and biochemical effects exerted by PI3K/mTOR inhibitors need to be compared across divergent preclinical GC models (e.g., intestinal and diffuse type). Compilation of a range of preclinical GC models in the one location would enable studies that assess subtype-specific inhibitor sensitivity and resistance. At this stage, however, these studies are limited due to the unavailability of a readily testable mouse model for diffuse-type GC.

STAT3 has long been recognized as a promising therapeutic target, but its function as a latent transcription factor and its close homology with other STAT family members has impeded the development of small molecular inhibitors for the clinic (62). Although targeting IL-6 has shown some promising results in a subset of patients with ovarian cancer (63), the extensive redundancies among IL-6 family cytokines and their wide-spread production is likely to limit the efficacy of targeting one single cytokine. Here, we revealed that GP130-mediated activation of the PI3K/mTORC1 pathway is required for inflammation-associated tumor promotion. Specifically, we have demonstrated the efficacy of the clinically approved mTORC1 inhibitor RAD001 in 2 inflammation-associated gastrointestinal tumor models. In both models, the efficacy of mTORC1 inhibition is comparable to genetic/pharmacological impairment of the parallel GP130/STAT3 signaling axis (10, 29). The surprising mTORC1 dependency of gastrointestinal tumors in mice suggests that clinically approved rapalogs, and/or inhibitors that target upstream kinases such as JAK and PI3K, may also effectively suppress inflammation-associated gastrointestinal tumor promotion in humans.

Methods

Mice, treatments, and reagents. Homozygous $gp130^{Y757F/Y757F}$ knockin mice ($gp130^{FF}$ mice) and their corresponding $gp130^{FF}Stat3^{+/-}$, $gp130^{FF}Stat1^{-/-}$, $gp130^{FF}Il6^{-/-}$, and $gp130^{FF}Il11ra^{-/-}$ compound mutant derivatives (10, 12, 13) as well as wild-type control mice were propagated on a mixed C57B6 × 129/Sv background. Age- and gender-matched mice were housed under specific pathogen–free conditions.

RAD001 (everolimus, a gift from Novartis) was diluted to 2% (w/w) in a microemulsion, which also served as the placebo control. To yield final dosages (3 mg/kg, 10 mg/kg), microemulsions were diluted in water prior to oral gavage for 5 days per week for 6 consecutive weeks. Recombinant human IL-6, hyper–IL-6 (37), and IL-11 were gifts from S. Rose-John (Christian-Albrechts-Universität zu Kiel, Kiel, Germany) and L. Robb (Walter and Eliza Hall Institute, Melbourne, Australia), and the IL-11 antagonist was from CSL Limited. Mice were challenged with single i.p. injections of IL-6 or IL-11 (5 μg diluted in PBS), the pan-JAK inhibitor AG490 (40 mg/kg, Sigma-Aldrich) or wortmannin (5 mg/kg, Sigma-Aldrich; both diluted in 45% DMSO/PBS), or were treated with the IL-11 antagonist (40 mg/kg) 3 times per week for 4 consecutive weeks.

CAC was induced and monitored by endoscopy as described previously (29, 30). Briefly, 6-week-old wild-type mice were injected once with 10 mg/kg azoxymethane (Sigma-Aldrich) and 7 days later received drinking water containing 1.5% (w/v) dextran sodium sulphate (MW = 36–50 kDa; MP Biomedicals) for 5 consecutive days, followed by 2 weeks of normal drinking water. This cycle was repeated once before colonic tumorigenesis was assessed by endoscopy, and the mice were randomized into 2 treatment groups based on their tumor scores.

Tissue collection and isolation of epithelial cells. Gastric or colonic tumors and adjacent antral or colon tissues were resected and weighed, and entire stomachs or colons were processed for histological analysis (10). To obtain gastric epithelial cells, antral mucosae or tumors were washed with PBS and incubated in 3 mM EDTA/0.5 mM DTT before vigorous shaking to mechanically release epithelial cells from the stroma.

Gene expression profiling and human GP130 gene signature. Whole-genome expression profiling was performed on MouseWG-6 v2.0 Expression BeadChips (Illumina), with 8 mice per group ($gp130^{FF}$ tumors, $gp130^{FF}$ adjacent unaffected tissue, and $gp130^{WT}$ antral tissue). Raw gene expression intensity values and detection *P* values were extracted using Illumina's Genome Studio. Probes with raw intensity values of less than 1 or detection *P* values of more than 0.05 across all samples were filtered out, followed by $\log_2$ transformation of raw intensity values. LIMMA (Linear Models for Microarray Data; ref. 64) was used to derive a GP130 mouse gene signature, consisting of probes that represent differentially expressed genes between $gp130^{WT}$ normal stomach and $gp130^{FF}$ tumors (false discovery rate < 1×10^{-5}). Using the table of mouse-human orthologous genes (ftp://ftp.informatics.jax.org/pub/reports/index.html), the GP130 mouse gene signature was translated into orthologous human gene symbols that were then mapped to the corresponding Affymetrix HGU133Plus_2 probe sets (Supplemental Table 1). The array data are available at the NCBI Gene Expression Omnibus repository (mouse gene expression profiles: GSE35808; human GC profiles: GSE15459 and GSE35809).

Protein extraction and immunoblot analysis. Protein lysates were prepared using the TissueLyser II (Qiagen) and RIPA lysis buffer (13) supplemented with protease and phosphatase inhibitor tablets (Roche). Lysates were separated by sodium dodecyl sulphate polyacrylamide gel electrophoresis (10) and transferred to nitrocellulose membranes by iBlot (Invitrogen). Proteins were visualized and quantified using the Odyssey Infrared Imaging System and quantification tools (LI-COR Biosciences) or the enhanced chemiluminescence detection system (ChemiDoc XRS+, Bio-Rad).

Histological and immunohistological analysis. General histology and immunohistochemical stainings were performed as described previously (10). In vivo proliferation was assessed by staining with anti-BrdU of tissues collected 2 hours after i.p. injection of 50 mg/kg BrdU (Amersham Biosciences, GE Healthcare). Apoptosis (Cell Death Detection Kit, Roche) and tissue hypoxia (60 mg/kg, Hypoxyprobe-1 Kit, Chemicon) stainings were performed as per the manufacturers' instructions.

Human tissues. Paraffin-embedded human GC biopsies were obtained from the Peter MacCallum Cancer Centre, with approval from the Research Ethics Review Committee and signed patient informed consent.

Cell cultures. Serum-starved cultures of 293T cells, grown and transiently transfected using FuGENE 6 (Roche) as described previously (13), were stimulated with hyper–IL-6 (100 ng/ml) or Epo (50 U/ml, Eprex, Janssen-Cilag) and, where indicated, pretreated with the PI3K inhibitor LY294002 (25 μM, Cell Signaling Technology) 60 minutes prior to cytokine stimulation. PI3K activity assays (36) were carried out in 293T cells that were plated at 2.5×10^5 cells per well on fibronectin-coated glass coverslips and cultured until they reached 80% confluency.

Statistics. Unless otherwise stated, comparisons between mean values were performed by ANOVA or a 2-tailed Student's *t* test as appropriate using Prism 5 software (GraphPad). A *P* value of less than 0.05 was considered statistically significant.

Study approval. All animal studies were approved and conducted in accordance with the Animal Ethics Committee of the Ludwig Institute for Cancer Research/University of Melbourne Department of Surgery. The human GC biopsies from deidentified patients were obtained with signed patient-informed consent and approval from the Research Ethics Review Committee of the Peter MacCallum Cancer Centre.

Further information is provided in the Supplemental Methods.

Acknowledgments

We thank Rachel Hughan, Christine Dijkstra, Elsbeth Richardson, Valarie Feakes, Cary Tsui, and the LICR animal facility staff for expert technical assistance. We thank Stefan Rose-John (Christian-Albrechts-Universität zu Kiel) for recombinant IL-6 and hyper–IL-6, Lorraine Robb (Walter and Eliza Hall Institute) for recombinant IL-11, and Nick Wilson (CSL Limited, Melbourne, Australia) for providing IL-11Rα–expressing BaF3 cells. We are grateful to Florian Greten and Joan Heath for helpful discussions. This work was supported by funds from the Operational Infrastructure Support Program provided by the Victorian Government (Australia) and the following grants from the National Health and Medical Research Council Australia (NHMRC): no. 433617, no. 487922, no. 603122, no. 603132, and no. 1008614. M. Ernst is a Senior Research Fellow of the NHMRC. Work of Michael Hallek was supported by Deutsche Forschungsgemeinschaft SFB 832 (A16). The contents of this material are solely the responsibility of the Administering Institution, Participating Institutions, or individual authors and do not reflect the views of NHMRC.

Received for publication June 27, 2012, and accepted in revised form November 27, 2012.

Address correspondence to: Matthias Ernst, Walter and Eliza Hall Institute for Medical Research, 1G Royal Parade, Parkville, Victoria 3052, Australia. Phone: 61.3.9345.2555; Fax: 61.3.9347.0852; E-mail: Matthias.Ernst@wehi.edu.au.

Stefan Thiem, Thomas P. Pierce, Michelle Palmieri, Tracy L. Putoczki, Michael Buchert, Adele Preaudet, Ryan O. Farid, Chris Love, and Matthias Ernst's present address is: Walter and Eliza Hall Institute for Medical Research, Parkville, Victoria, Australia.

Bruno Catimel's present address is: Ludwig Institute for Cancer Research, Melbourne-Austin Branch, Heidelberg, Victoria, Australia.

Andrew Jarnicki's present address is: University of Newcastle, Newcastle, New South Wales, Australia.

1. Grivennikov SI, Greten FR, Karin M. Immunity, inflammation, and cancer. *Cell*. 2010;140(6):883–899.
2. Bernstein CN, Blanchard JF, Kliewer E, Wajda A. Cancer risk in patients with inflammatory bowel disease: a population-based study. *Cancer*. 2001;91(4):854–862.
3. Ekbom A, Helmick C, Zack M, Adami HO. Ulcerative colitis and colorectal cancer. A population-based study. *N Engl J Med*. 1990;323(18):1228–1233.
4. Flossmann E, Rothwell PM. Effect of aspirin on long-term risk of colorectal cancer: consistent evidence from randomised and observational studies. *Lancet*. 2007;369(9573):1603–1613.
5. Cuzick J, et al. Aspirin and non-steroidal anti-inflammatory drugs for cancer prevention: an international consensus statement. *Lancet Oncol*. 2009;10(5):501–507.
6. Yu H, Kortylewski M, Pardoll D. Crosstalk between cancer and immune cells: role of STAT3 in the tumour microenvironment. *Nat Rev Immunol*. 2007;7(1):41–51.
7. Jarnicki A, Putoczki T, Ernst M. Stat3: linking inflammation to epithelial cancer - more than a "gut" feeling? *Cell Div*. 2010;5:14.
8. Heinrich PC, Behrmann I, Haan S, Hermanns HM, Muller-Newen G, Schaper F. Principles of interleukin (IL)-6-type cytokine signalling and its regulation. *Biochem J*. 2003;374(Pt 1):1–20.
9. Nakayama T, et al. Expression of interleukin-11 (IL-11) and IL-11 receptor alpha in human gastric carcinoma and IL-11 upregulates the invasive activity of human gastric carcinoma cells. *Int J Oncol*. 2007;30(4):825–833.
10. Ernst M, et al. STAT3 and STAT1 mediate IL-11-dependent and inflammation-associated gastric tumorigenesis in gp130 receptor mutant mice. *J Clin Invest*. 2008;118(5):1727–1738.
11. Park EJ, et al. Dietary and genetic obesity promote liver inflammation and tumorigenesis by enhancing IL-6 and TNF expression. *Cell*. 2010; 140(2):197–208.
12. Tebbutt NC, et al. Reciprocal regulation of gastrointestinal homeostasis by SHP2 and STAT-mediated trefoil gene activation in gp130 mutant mice. *Nat Med*. 2002;8(10):1089–1097.
13. Jenkins BJ, et al. Hyperactivation of Stat3 in gp130 mutant mice promotes gastric hyperproliferation and desensitizes TGF-beta signaling. *Nat Med*. 2005;11(8):845–852.
14. Putoczki T, Ernst M. More than a sidekick: the IL-6 family cytokine IL-11 links inflammation to cancer. *J Leukoc Biol*. 2010;88(6):1109–1117.
15. Easton JB, Houghton PJ. mTOR and cancer therapy. *Oncogene*. 2006;25(48):6436–6446.
16. Shaw RJ, Cantley LC. Ras, PI(3)K, and mTOR signalling controls tumour cell growth. *Nature*. 2006;441(7092):424–430.
17. Faivre S, Kroemer G, Raymond E. Current development of mTOR inhibitors as anticancer agents. *Nat Rev Drug Discov*. 2006;5(8):671–688.
18. Agarwala SS, Case S. Everolimus (RAD001) in the treatment of advanced renal cell carcinoma: a review. *Oncologist*. 2010;15(3):236–245.
19. Chen C, Liu Y, Zheng P. Mammalian target of rapamycin activation underlies HSC defects in autoimmune disease and inflammation in mice. *J Clin Invest*. 2010;120(11):4091–4101.
20. Deng L, et al. A novel mouse model of inflammatory bowel disease links mammalian target of rapamycin-dependent hyperproliferation of colonic epithelium to inflammation-associated tumorigenesis. *Am J Pathol*. 2010;176(2):952–967.
21. Lauren P. The two histological main types of gastric carcinoma: diffuse and so-called intestinal-type carcinoma. An attempt at a histo-clinical classification. *Acta Pathol Microbiol Scand*. 1965;64:31–49.
22. Boussioutas A, et al. Distinctive patterns of gene expression in premalignant gastric mucosa and gastric cancer. *Cancer Res*. 2003;63(10):2569–2577.
23. Carvalho CM, Chang J, Lucas JE, Nevins JR, Wang Q, West M. High-dimensional sparse factor modeling: applications in gene expression genomics. *J Am Stat Assoc*. 2008;103(484):1438–1456.
24. Ooi CH, et al. Oncogenic pathway combinations predict clinical prognosis in gastric cancer. *PLoS Genet*. 2009;5(10):e1000676.
25. Judd LM, et al. Gastric cancer development in mice lacking the SHP2 binding site on the IL-6 family co-receptor gp130. *Gastroenterology*. 2004;126(1):196–207.
26. Jenkins BJ, et al. Pathologic consequences of STAT3 hyperactivation by IL-6 and IL-11 during hematopoiesis and lymphopoiesis. *Blood*. 2007;109(6):2380–2388.
27. Wander SA, Hennessy BT, Slingerland JM. Next-generation mTOR inhibitors in clinical oncology: how pathway complexity informs therapeutic strategy. *J Clin Invest*. 2011;121(4):1231–1241.
28. O'Reilly KE, et al. mTOR inhibition induces upstream receptor tyrosine kinase signaling and activates Akt. *Cancer Res*. 2006;66(3):1500–1508.
29. Bollrath J, et al. gp130-mediated Stat3 activation in enterocytes regulates cell survival and cell-cycle progression during colitis-associated tumorigenesis. *Cancer Cell*. 2009;15(2):91–102.
30. Becker C, Fantini MC, Neurath MF. High resolution colonoscopy in live mice. *Nat Protoc*. 2006;1(6):2900–2904.
31. Fujishita T, Aoki K, Lane HA, Aoki M, Taketo MM. Inhibition of the mTORC1 pathway suppresses intestinal polyp formation and reduces mortality in ApcDelta716 mice. *Proc Natl Acad Sci U S A*. 2008;105(36):13544–13549.
32. Holash J, et al. Vessel cooption, regression, and growth in tumors mediated by angiopoietins and VEGF. *Science*. 1999;284(5422):1994–1998.
33. Etoh T, Inoue H, Tanaka S, Barnard GF, Kitano S, Mori M. Angiopoietin-2 is related to tumor angiogenesis in gastric carcinoma: possible in vivo regulation via induction of proteases. *Cancer Res*. 2001;61(5):2145–2153.
34. Hudson CC, et al. Regulation of hypoxia-inducible factor 1alpha expression and function by the mammalian target of rapamycin. *Mol Cell Biol*. 2002;22(20):7004–7014.
35. Niu G, et al. Constitutive Stat3 activity up-regulates VEGF expression and tumor angiogenesis. *Oncogene*. 2002;21(13):2000–2008.
36. Palmieri M, et al. Analysis of cellular phosphatidylinositol (3,4,5)-trisphosphate levels and distribution using confocal fluorescent microscopy. *Anal Biochem*. 2010;406(1):41–50.
37. Fischer M, et al. I. A bioactive designer cytokine for human hematopoietic progenitor cell expansion. *Nat Biotechnol*. 1997;15(2):142–145.
38. Vanhaesebroeck B, Guillermet-Guibert J, Graupera M, Bilanges B. The emerging mechanisms of isoform-specific PI3K signalling. *Nat Rev Mol Cell Biol*.

2010;11(5):329–341.
39. Gharbi SI, et al. Exploring the specificity of the PI3K family inhibitor LY294002. *Biochem J*. 2007;404(1):15–21.
40. Gustafson AM, et al. Airway PI3K pathway activation is an early and reversible event in lung cancer development. *Sci Transl Med*. 2010;2(26):26ra25.
41. Al-Batran SE, Ducreux M, Ohtsu A. mTOR as a therapeutic target in patients with gastric cancer. *Int J Cancer*. 2012;130(3):491–496.
42. Hollander MC, Blumenthal GM, Dennis PA. PTEN loss in the continuum of common cancers, rare syndromes and mouse models. *Nat Rev Cancer*. 2011;11(4):289–301.
43. Rebouissou S, et al. Frequent in-frame somatic deletions activate gp130 in inflammatory hepatocellular tumours. *Nature*. 2009;457(7226):200–204.
44. Pilati C, et al. Somatic mutations activating STAT3 in human inflammatory hepatocellular adenomas. *J Exp Med*. 2011;208(7):1359–1366.
45. Jeong EG, et al. Somatic mutations of JAK1 and JAK3 in acute leukemias and solid cancers. *Clin Cancer Res*. 2008;14(12):3716–3721.
46. Constantinescu SN, Girardot M, Pecquet C. Mining for JAK-STAT mutations in cancer. *Trends Biochem Sci*. 2008;33(3):122–131.
47. He B, et al. SOCS-3 is frequently silenced by hypermethylation and suppresses cell growth in human lung cancer. *Proc Natl Acad Sci U S A*. 2003;100(24):14133–14138.
48. Greten FR, et al. IKKbeta links inflammation and tumorigenesis in a mouse model of colitis-associated cancer. *Cell*. 2004;118(3):285–296.
49. Grivennikov S, et al. IL-6 and Stat3 are required for survival of intestinal epithelial cells and development of colitis-associated cancer. *Cancer Cell*. 2009;15(2):103–113.
50. Naugler WE, et al. Gender disparity in liver cancer due to sex differences in MyD88-dependent IL-6 production. *Science*. 2007;317(5834):121–124.
51. Nishimoto N, Kishimoto T. Interleukin 6: from bench to bedside. *Nat Clin Pract Rheumatol*. 2006;2(11):619–626.
52. Doi T, et al. Multicenter phase II study of everolimus in patients with previously treated metastatic gastric cancer. *J Clin Oncol*. 2010;28(11):1904–1910.
53. Van Cutsem E, et al. Phase 3 trial of everolimus in previously treated patients with advanced gastric cancer: GRANITE-1. *J Clin Oncol*. 2012; 30(suppl 4; abstr LBA3).
54. Altomare I, et al. A phase II trial of bevacizumab plus everolimus for patients with refractory metastatic colorectal cancer. *Oncologist*. 2011; 16(8):1131–1137.
55. Muranen T, et al. Inhibition of PI3K/mTOR leads to adaptive resistance in matrix-attached cancer cells. *Cancer Cell*. 2012;21(2):227–239.
56. Takahashi-Tezuka M, et al. Gab1 acts as an adapter molecule linking the cytokine receptor gp130 to ERK mitogen-activated protein kinase. *Mol Cell Biol*. 1998;18(7):4109–4117.
57. Pfeffer LM, Mullersman JE, Pfeffer SR, Murti A, Shi W, Yang CH. STAT3 as an adapter to couple phosphatidylinositol 3-kinase to the IFNAR1 chain of the type I interferon receptor. *Science*. 1997;276(5317):1418–1420.
58. Yokogami K, Wakisaka S, Avruch J, Reeves SA. Serine phosphorylation and maximal activation of STAT3 during CNTF signaling is mediated by the rapamycin target mTOR. *Curr Biol*. 2000;10(1):47–50.
59. Oh H, et al. Activation of phosphatidylinositol 3-kinase through glycoprotein 130 induces protein kinase B and p70 S6 kinase phosphorylation in cardiac myocytes. *J Biol Chem*. 1998; 273(16):9703–9710.
60. Weigert C, et al. Direct cross-talk of interleukin-6 and insulin signal transduction via insulin receptor substrate-1 in skeletal muscle cells. *J Biol Chem*. 2006;281(11):7060–7067.
61. Engelman JA. Targeting PI3K signalling in cancer: opportunities, challenges and limitations. *Nat Rev Cancer*. 2009;9(8):550–562.
62. Mankan AK, Greten FR. Inhibiting signal transducer and activator of transcription 3: rationality and rationale design of inhibitors. *Expert Opin Investig Drugs*. 2011;20(9):1263–1275.
63. Coward J, et al. Interleukin-6 as a therapeutic target in human ovarian cancer. *Clin Cancer Res*. 2011;17(18):6083–6096.
64. Smyth GK. Linear models and empirical bayes methods for assessing differential expression in microarray experiments. *Stat Appl Genet Mol Biol*. 2004;3:Article3.